Proton Distribution Radii of ^{12–19}C Illuminate Features of Neutron Halos

R. Kanungo *et al.*

Phys. Rev. Lett. **117**, 102501 — Published 2 September 2016
DOI: 10.1103/PhysRevLett.117.102501

Proton distribution radii of $^{12-19}$C illuminate features of neutron halos

R. Kanungo[1], W. Horiuchi[2], G. Hagen[3,4*], G. R. Jansen[5,3*], P. Navratil[6], F. Ameil[7], J. Atkinson[1], Y. Ayyad[8], D. Cortina-Gil[8], I. Dillmann[7†], A. Estradé[1,7], A. Evdokimov[7], F. Farinon[7], H. Geissel[7,9], G. Guastalla[7], R. Janik[10], M. Kimura[2], R. Knöbel[7], J. Kurcewicz[7], Yu. A. Litvinov[7], M. Marta[7], M. Mostazo[8], I. Mukha[7], C. Nociforo[7], H.J. Ong[11], S. Pietri[7], A. Prochazka[7], C. Scheidenberger[7,9], B. Sitar[10], P. Strmen[10], Y. Suzuki[11,12], M. Takechi[7], J. Tanaka[13], I. Tanihata[13,14], S. Terashima[14], J. Vargas[8], H. Weick[7], J. S. Winfield[7]

[1]*Astronomy and Physics Department, Saint Mary's University, Halifax, NS B3H 3C3, Canada*
[2]*Department of Physics, Hokkaido University, Sapporo 060-0810, Japan*
[3]*Physics Division, Oak Ridge National Laboratory, Oak Ridge, TN 37831, USA*
[4]*Department of Physics and Astronomy, University of Tennessee, Knoxville, TN 37996, USA*
[5]*National Center for Computational Sciences, Oak Ridge National Laboratory, Oak Ridge, TN 37831 USA*
[6]*TRIUMF, Vancouver, BC V6T 4A3, Canada*
[7]*GSI Helmholtzzentrum für Schwerionenforschung, D-64291 Darmstadt, Germany*
[8]*Universidad de Santiago de Compostela, E-15706 Santiago de Compostella, Spain*
[9]*Justus-Liebig University, 35392 Giessen, Germany*
[10]*Faculty of Mathematics and Physics, Comenius University, 84215 Bratislava, Slovakia*
[11]*Department of Physics, Niigata University, Niigata 950-2181, Japan*
[12]*RIKEN Nishina Center, Wako, Saitama 351-0198, Japan*
[13]*RCNP, Osaka University, Mihogaoka, Ibaraki, Osaka 567 0047, Japan and*
[14]*School of Physics and Nuclear Energy Engineering and IRCNPC, Beihang University, Beijing 100191, China*

(Dated: August 10, 2016)

Proton radii of $^{12-19}$C densities derived from first accurate charge changing cross section measurements at 900*A* MeV with a carbon target are reported. A thick neutron surface evolves from $\sim$ 0.5 fm in ^{15}C to $\sim$ 1 fm in ^{19}C. The halo radius in ^{19}C is found to be 6.4±0.7 fm as large as ^{11}Li. *Ab initio* calculations based on chiral nucleon-nucleon and three-nucleon forces reproduce well the radii.

PACS numbers: 21.10.Gv, 21.10.Ft, 21.60.De, 25.60.-t, 25.60.Dz

The existence of thick neutron skins and halos [1–3] in neutron-rich nuclei has brought a dramatic change in our view of the nucleus. These unexpected features are exhibited through formation of neutron dominated nuclear surfaces and hence large root mean square point matter radii (R_m). The knowledge on how root mean square point proton distribution radii, henceforth in the article referred to as proton radii (R_p), evolve with neutron excess is still extremely limited. Proton radii are crucial for deriving the neutron skin (surface) thickness and understanding the spatial correlation between halo neutrons and its core-nucleus. Proton radii can also provide knowledge on shell structure evolution, as recently discussed for ^{52}Ca [4]. The neutron skin may also be related to the symmetry energy (S_v) and its density derivative at saturation density (L) defining the EOS of asymmetric nuclear matter [5].

Here we report the first precise determination of proton radii of neutron-rich isotopes $^{15-19}$C from the measurement of charge changing cross sections that show rapidly growing thick neutron surfaces approaching the neutron drip line. The proton radii derived for $^{12-14}$C are in agreement with those obtained from traditional methods such as electron scattering without any scaling factor. This clearly established the present technique as a valuable method to determine the proton radii of very neutron-rich isotopes. The measured radii are in good agreement with those computed using *ab initio* coupled-cluster theory based on chiral nucleon-nucleon and three-nucleon interactions [6].

The carbon isotopes draw interest because their R_m show large enhancements for ^{15,19}C [7] and ^{22}C [8, 9]. This signals the presence of neutron halos. It is interesting to see how such structure evolution of neutron-rich C isotopes affects their proton distribution.

Electron-nucleus scattering and measurement of muonic X-rays are used to determine the charge radii (R_c) of stable nuclei. The R_c of ^{12}C from e$^-$ scattering was found to be 2.478±0.009 fm [10] which is consistent with 2.472±0.015 fm from muonic X ray studies [11]. For ^{13}C, the weighted average of two e$^-$ scattering measurements [12, 13] yields R_c = 2.43±0.02 fm, while the muonic X-ray measurements [11, 14] find R_c =2.463±0.004 fm. Results from e$^-$ scattering of ^{14}C gives R_c =2.56±0.05 fm [15], which is in agreement with

*This manuscript has been authored by UT-Battelle, LLC under Contract No. DE-AC05-00OR22725 with the U.S. Department of Energy. The United States Government retains and the publisher, by accepting the article for publication, acknowledges that the United States Government retains a non-exclusive, paid-up, irrevocable, world-wide license to publish or reproduce the published form of this manuscript, or allow others to do so, for United States Government purposes. The Department of Energy will provide public access to these results of federally sponsored research in accordance with the DOE Public Access Plan (http://energy.gov/downloads/doe-public-access-plan)
†Present address : TRIUMF, Vancouver, Canada

2.496±0.019 fm from muonic X-ray measurements.

At present these techniques cannot be used for neutron-rich carbon isotopes. A new approach, used in this work, is to measure the charge changing cross section (σ_{cc}) and derive the point proton radius (R_p) from it using the finite-range Glauber model. This method has been employed in Refs.[16, 17] and with zero-range calculations in Ref.[18]. The effect of proton evaporation from neutron removal cross sections to states above the proton threshold is negligibly small for $^{12-19}$C since these nuclei are not in the vicinity of any proton unbound isotopes and the proton separation energies are fairly large. At beam energies ∼900A MeV, nuclear inelastic excitation cross section to states above the proton emission threshold is also negligibly small. The above effects become relevant for correction for nuclei at or neighbouring the proton drip-line.

The first precise measurements of charge changing cross sections and hence R_p of neutron-rich isotopes $^{15-19}$C as well as for $^{12-14}$C are reported here. The experiment was performed using the fragment separator FRS [19] at GSI, Darmstadt, Germany. The carbon isotopes were produced through fragmentation of 1A GeV primary beams of ^{20}Ne and ^{40}Ar interacting with a 6.3 g/cm^2 thick Be target. The isotopes of interest were separated, identified, and counted using event-by-event information of magnetic rigidity (Bρ), time-of-flight (TOF), and energy-loss (ΔE). A multi-sampling ionization chamber (MUSIC) [20] provides the Z identification from ΔE. Figure 1 shows the experiment setup. The first three (F1, F2 and F3), focal planes of the FRS are dispersive while the final one, F4, is achromatic, where the reaction target, C (4.01 g/cm^2) was placed. The energies of the isotopes at the reaction target were ∼900A MeV and are listed in Table 1. Plastic scintillator detectors placed at the mid-plane F2 and before the reaction target at F4 measured the time-of-flight of the incoming beam. The scintillator before the target at F4 was used as the trigger of the data acquisition system. Two position sensitive time projection chambers (TPC) [21] were placed before the target at F4 which provided beam tracking defining the beam profile on the target. In addition, TPCs were also placed at F2. The position information in combination with the central magnetic rigidity of the dipoles was used to determine event by event Bρ of the incident particle.

The σ_{cc} is measured using the transmission technique, where the number (N_{in}) of incident nuclei ^AZ, before the reaction target is identified and counted. After the target, the nuclei with the same charge Z are identified and counted event by event (N_{sameZ}). The σ_{cc} is obtained from a ratio of these counts and is defined as $\sigma_{cc} = t^{-1}\ln\big(T_{t_{out}}/T_{t_{in}}\big)$ where $T = N_{sameZ}/N_{in}$, t_{in} and t_{out} refer to measurements with and without the reaction target, t is the thickness of the target.

A restricted position and angle selection of the beam on target eliminated spurious effects of losses due to large angle scattering out of the detector acceptance. A veto scintillator was placed before the target with a central hole of a size smaller than the target. This rejected scattered events from upstream matter and multi-hit events where one of the particles can miss hitting a MUSIC giving incorrect reaction information. The particle identification condition of the incident beam was defined in a way such that the contamination level from Z=5 and 7 beam events relative to Z=6 is ≤10^{-4}.

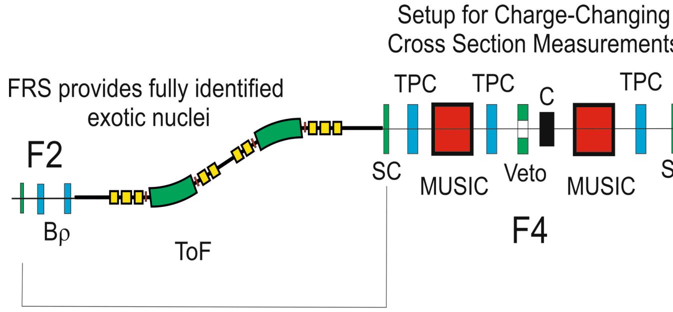

FIG. 1: Schematic view of the experiment setup at the FRS with detector arrangement at the final focus F4.

After the reaction target the beam events with Z=6 were counted using the second MUSIC. The energy-loss values of the TPC and the plastic scintillator detectors placed after the target provided additional information to ensure proper Z identification and counting. The resolution of the MUSIC for Z=6 was ΔZ (in σ) = 0.12. The selection window covered ∼ ±4σ of the Z=6 particles.

With the desired isotope of C selected as the incoming beam, the production of Z=7 events after the target is from charge exchange or proton transfer reactions where one proton is added to the nucleus. This cross section therefore does not involve reactions with the protons in the C isotope and is hence subtracted to derive the measured charge changing cross section. While this cross section is generally very small (<1 mb), for the neutron-rich C isotopes it was found to be a few mb [22].

The measured values of σ_{cc} are listed in Table 1. The cross section increases for ^{15}C which has a halo structure and continues gradually increasing for ^{16,17}C. This is unlike Ref.[18], reporting the σ_{cc} of ^{16}C to be smaller than ^{15}C. With the halo-effect of ^{15}C one would expect a small increase in the proton radius as seen for example for ^{11}Be [23]. A large increase in σ_{cc} is not found for ^{19}C although it is a halo nucleus. This is because the effect of the center of mass motion of the halo on the proton radius becomes smaller with larger mass number than in ^{11}Be. The σ_{cc} for $^{12-20}$C reported in Ref.[24] with large uncertainties are systematically higher than those in [25] for stable isotopes and not consistent with R_p from e$^-$ scattering.

The finite-range Glauber model [26] with harmonic oscillator density is used for deriving the R_p from the σ_{cc}. The R_p are listed in Table 1. The charge radii of $^{12-14}$C known from e$^-$- scattering and muonic X-ray measurements are used to find the respective R_p (blue diamonds

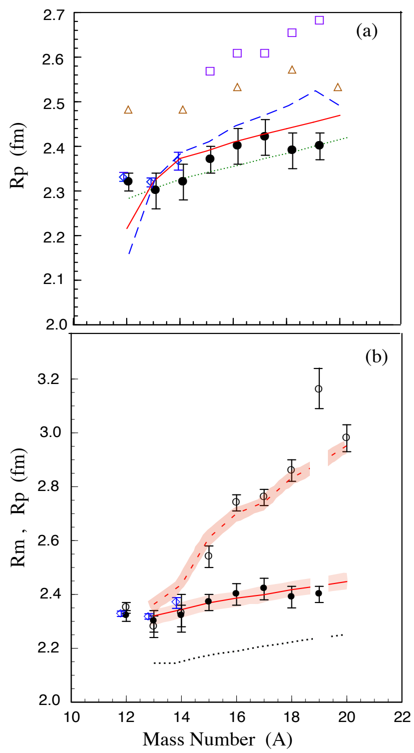

FIG. 2: R_p extracted from σ_{cc} for $^{12-19}$C (black filled circles). The blue open diamonds are R_p from e^--scattering and muonic X-rays for $^{12-14}$C. (a) The relativistic mean field theory calculations with spherical/deformed potentials are shown by the red solid line/ blue dashed line. The green dotted line shows results of Hartree Fock calculations. The AMD results are shown by open triangles [27] and open squares [28]. (b) The R_m from the present analysis of σ_I [7] are shown by black open circles. The results of coupled cluster calculations are shown for R_p as solid (red) and dotted (black) lines using the chiral NNLO$_{\rm sat}$ interaction and the nucleon-nucleon interaction NNLO$_{\rm opt}$ [29], respectively. The matter radii with NNLO$_{\rm sat}$ is shown by the red dashed line. The shaded bands show the predicted uncertainty.

in Fig.2 and $R_p^{(e^-,\mu)}$ in Table 1) following the formula in Ref.[23]. A good agreement is seen with the R_p found in this work. This lends strong support to this technique of successfully extracting R_p from σ_{cc}. No scaling factor of σ_{cc} was required for this agreement as was also seen in Ref.[16], unlike the discussion in Ref.[18].

The matter radii of $^{12-19}$C shown in Fig.2b (open circles) are derived in this work from a finite-range Glauber model [30] analysis of the interaction cross section (σ_I) data from Ref.[7]. In this analysis the R_p are fixed to the values from Table 1 while the neutron radii are varied to reproduce the (σ_I) data. The matter radius of ^{20}C is shown from Ref.[7]. The combined information from proton radii and matter radii allow to fully characterize the halo features of ^{15,19}C. In a core plus neutron model following Ref.[3], the halo radius, R$_h$, of $\sim$ 6.4$\pm$0.7 fm for ^{19}C derived in this work shows the presence of a more prominent halo in this nucleus compared to $\sim$ 4.2$\pm$0.5 fm for ^{15}C. The root mean square distance between the center of mass of the core and the halo neutron R_{c-n} using the method in Ref.[3] for ^{15}C is 7.2 $\pm$ 4.0 fm derived using R_p and 4.15 $\pm$ 0.5 fm using R_m. For ^{19}C it is 4.1 $\pm$ 10 fm using R_p and 6.6 $\pm$ 0.5 fm using R_m. The radius of the valence neutron was deduced to be 5.5$\pm$0.3 fm from Coulomb dissociation of ^{19}C [31].

The R_p predicted by the relativistic mean field theory [32] using the NL3 parameters in a spherical potential is in overall agreement (Fig. 2a) with the R_p of $^{13-17}$C and slightly higher for ^{18,19}C. Those with a non-spherical potential predict slightly higher radii for $^{14-19}$C. The radii predicted in the framework of microscopic non-relativistic Hartree-Fock method with a hybrid of Gogny and Skyrme effective interactions is in agreement with the data of some isotopes [32]. The radii calculated in the Antisymmetrized Molecular Dynamics (AMD) framework Fig.2a greatly overpredict the data (open triangles [27]) and (open squares [28]).

We also perform coupled-cluster computations for the radii and compare with data. For the closed (sub-)shell nucleus ^{14}C we use the coupled-cluster method with singles-and-doubles excitations [33] to compute the expectation value of the intrinsic point-proton and neutron radii. To access the open-shell nuclei ^{13,15}C we use particle-removed/attached equation-of-motion coupled-cluster method [34, 35], while for $^{16-19}$C we employ the recently developed coupled-cluster effective interaction (CCEI) method in the *sd* shell [36, 37]. To compute the intrinsic radii of $^{16-19}$C within CCEI we follow the scheme outlined in Ref.[36], and include the core and one-body parts of the valence-space radius operator, while we neglect the two-body part. We solve our coupled-cluster equations using a Hartree-Fock basis built from a harmonic-oscillator basis consisting of fifteen major oscillator shells ($N_{\rm max} = 2n + l = 14$) with the additional energy cut $E_{3\rm max} = N_1 + N_2 + N_3 \leq 16$ for the three-nucleon interaction. Here $N_i = 2n_i + l_i$ refers to the major oscillator shell of the i^{th} particle. For the computed radii we estimate an uncertainty of $\pm$0.04 fm coming from the model-space and coupled-cluster method.

We perform our coupled-cluster calculations using various state-of-the-art chiral interactions. First, we focus on NNLO$_{\rm sat}$ which was obtained using a novel optimization strategy that simultaneously optimized the low-energy constants in the nucleon-nucleon (NN) and three-nucleon (3NF) sector at next-to-next-to leading order (NNLO) including data on charge radii and binding energies of selected nuclei up to ^{25}O in the fit [38]. NNLO$_{\rm sat}$ was recently successfully applied to compute radii of ^{48}Ca [6], and is for the first time employed for $^{13-19}$C in this work. Fig. 2b shows a comparison between data and coupled-cluster computations using NNLO$_{\rm sat}$ for the point-proton and matter radii of $^{13-19}$C. In addition to NNLO$_{\rm sat}$ we also compare data with the chiral interaction NNLO$_{\rm opt}$ [29] which does not include 3NFs. We observe that NNLO$_{\rm sat}$ gives overall good agreement

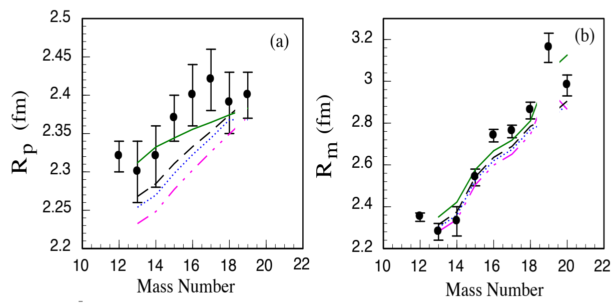

FIG. 3: The comparison of data with coupled cluster predictions for (a) proton radii (b) matter radii. The chiral interactions [39] are EM1 (dotted blue curve), EM3 (dashed double-dotted pink curve), EM4 (dashed black curve) and EM5 (solid green curve).

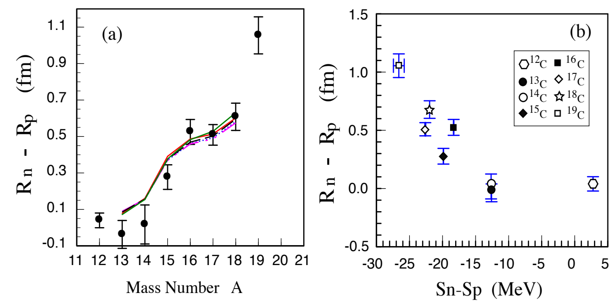

FIG. 4: (a) The measured neutron skin thickness for $^{12-19}$C compared to predictions using the different interactions, NNLO$_{\rm sat}$ (red solid curve), EM1 (dotted blue curve), EM3 (dashed double-dotted pink curve), EM4 (dashed black curve) and EM5 (solid green curve).(b) The measured neutron skin thickness variation with $S_n - S_p$ for $^{12-19}$C.

with data, while NNLO$_{\rm opt}$ significantly underestimates the radii. It is seen that the effects of simultaneously optimizing the low-energy coupling constants in the NN and three-nucleon sector, the inclusion of binding energies and radii of selected nuclei with $A \leq 25$ in the objecive function, and the inclusion of 3NFs with non-local regulators are indeed very significant and crucial for reproducing the measured proton radii. The results for the matter radii (Fig.2b dashed red curve) using NNLO$_{\rm sat}$ are also in good agreement with the data. Since ^{19}C is a weakly bound nucleus and the coupling to the particle continuum is not included in these calculations the CCEI result with NNLO$_{\rm sat}$ leads to ^{19}C being unbound. For this reason the radius is not defined and not shown in Fig. 2.

With the successful description of the radii in the coupled cluster framework using the NNLO$_{\rm sat}$ interaction, we now investigate how the data compares to a set of other chiral interactions. These interactions are adopted from Ref.[39] and include NN and 3NFs. The NN interactions are based on a similarity renormalization group transformation [40] of the chiral interaction at N^{3}LO from Ref. [41] and with a non-local 3NF at N^{2}LO. In contrast to NNLO$_{\rm sat}$ the low-energy coupling constants were determined from a fit to scattering data, binding energies and radii of nuclei with $A \leq 4$. The different forces used have different NN / 3NF cutoffs, namely EM1 = 2.0 fm^{-1} / 2.0 fm^{-1}, EM3 = 1.8 fm^{-1} / 2.0 fm^{-1}, EM4= 2.2 fm^{-1} / 2.0 fm^{-1}, EM5 = 2.8 fm^{-1} / 2.0 fm^{-1}. Fig. 3a and Fig. 3b compare the data of proton radii and matter radii, respectively, with predictions using these interactions that are shown as EM1 (dotted blue curve), EM3 (dashed double-dotted pink curve), EM4 (dashed black curve) and EM5 (solid green curve). It is seen that the agreement with the data over the different isotopes with the NNLO$_{\rm sat}$ is much better than any of the "EM" interactions. The R_p for $^{13-17}$C are not reproduced by the EM3 interaction. The EM1 and EM4 interactions do not reproduce the measured R_p for $^{15-17}$C. The interactions with a lower NN cutoff seems to predict smaller radii values. The agreement of the predictions with the matter radii (Fig. 3b) is better using the EM5 interaction than the other "EM" interactions, though once again the NNLO$_{\rm sat}$ predictions seem to be in much better agreement overall. This suggests that the NNLO$_{\rm sat}$ interaction has a better predictive capability for bulk properties of nuclei such as nuclear radii.

The neutron skin thickness defined as the difference of point neutron radius (R_n) and R_p is shown in Fig.4a. The red curve shows the coupled cluster calculations with the NNLO$_{\rm sat}$ interaction to be in good agreement with the data. The predictions with the other interactions are all very similar to each other and to that with the NNLO$_{\rm sat}$ interaction. We see a very thick neutron skin developing with increasing neutron-proton asymmetry. In Fig. 4b the relationship of the neutron skin thickness as a function of the difference between the one-neutron separation energy (S_n) and one-proton separation energy (S_p) is shown. The observed strong correlation observed in Fig. 4b points to a thick neutron skin (surface) being associated with the large Fermi-level difference of neutrons and protons, that occurs as nuclei become highly neutron-rich.

In summary, the first accurate determination of R_p of $^{12-19}$C is accomplished from charge changing cross section (σ_{cc}) measurements with a carbon target at 900A MeV. The Glauber model successfully relates the σ_{cc} to R_p which is seen from their agreement with radii from electron scattering. The radii are in overall good agreement with coupled-cluster computations using the chiral interaction NNLO$_{\rm sat}$.

The authors are thankful for the support of the GSI accelerator staff and the FRS technical staff for an efficient running of the experiment. The support from NSERC, Canada for this work is gratefully acknowledged. R. Kanungo thankfully acknowledges the HIC-for-FAIR program and JLU-Giessen for supporting part of the research stay. The support of the PR China government and Beihang university under the Thousand Talent program is gratefully acknowledged. The experiment is partly supported by the grant-in-aid program

TABLE I: Secondary beam energies, measured σ_{cc} and the root mean square proton and matter radii derived from the data for the carbon isotopes.

Isotope	E/A (MeV)	σ_{cc}^{ex} (mb)	R_p^{ex} (fm)	$R_p^{(e^-,\mu)}$ (fm)	R_m^{ex} (fm)
^{12}C	937	733(7)	2.32(2)	2.33(1)	2.35(2)
^{13}C	828	726(7)	2.30(4)	2.32(1)	2.28(4)
^{14}C	900	731(7)	2.32(4)	2.37(2)	2.33(7)
^{15}C	907	743(7)	2.37(3)		2.54(4)
^{16}C	907	748(7)	2.40(4)		2.74(3)
^{17}C	979	754(7)	2.42(4)		2.76(3)
^{18}C	895	747(7)	2.39(4)		2.86(4)
^{19}C	895	749(9)	2.40(3)		3.16(7)

of the Japanese government under the contract number 23224008. This work was supported by the Office of Nuclear Physics, U.S. Department of Energy (Oak Ridge National Laboratory), DE-SC0008499 (NUCLEI SciDAC collaboration), NERRSC Grant No. 491045-2011, and the Field Work Proposal ERKBP57 at Oak Ridge National Laboratory. Computer time was provided by the Innovative and Novel Computational Impact on Theory and Experiment (INCITE) program. TRIUMF receives funding via a contribution through the National Research Council Canada. This research used resources of the Oak Ridge Leadership Computing Facility located in the Oak Ridge National Laboratory, which is supported by the Office of Science of the Department of Energy under Contract No. DE-AC05-00OR22725, and used computational resources of the National Center for Computational Sciences and the National Institute for Computational Sciences.

[1] I. Tanihata *et al.*, Phys. Rev. Lett. **55**, 2676 (1985).
[2] P.G. Hansen and B. Jonson, Euro. Phys. Lett. **4**, 409 (1987).
[3] I. Tanihata *et al.*, Prog. Part. Nucl. Phys. **68**, 215 (2013).
[4] R. F. Garcia Ruiz *et al*, Nature Physics (2016), doi:10.1038/nphys3645
[5] J. M. Lattimer, Ann. Rev. Nucl. Part. Sci. **62**, 485 (2012)
[6] G. Hagen *et al.*, Nature Physics **12**, 186 (2016).
[7] A. Ozawa, T. Suzuki and I. Tanihata, Nucl. Phys. **A 693**, 32 (2001).
[8] W. Horiuchi and Y. Suzuki, Phys. Rev. **C 74**, 034311 (2006).
[9] K. Tanaka *et al.*, Phys. Rev. Lett. **104**, (2010) 062701.
[10] E.A.J.M. Offerman *et al.*, Phys. Rev. **C 44**, 1096 (1991).
[11] L.A. Schaller *et al.*, Nucl. Phys. **A 379**, 523 (1982).
[12] J. Heisenberg *et al.*, Nucl. Phys. **A 157**, 435 (1970).
[13] H.A. Bentz *et al.*, Z. Phys. **A 243**, 138 (1971).
[14] F.W.N. De Boer *et al.*, Nucl. Phys. **A 379**, 523 (1982).
[15] F.J. Kline *et al.*, Nucl. Phys. **A 209**, 381 (1973).
[16] A. Estrade *et al.*, Phys. Rev. Lett. **113**, 132501 (2014).
[17] S. Terashima *et al.*. Prog. in Theor. Exp. Phys., 101D02, (2014).
[18] T. Yamaguchi *et al.*, Phys. Rev. Lett. **107**, 032502 (2011).
[19] H. Geissel *et al.*, Nucl. Instrm. and Meth. in Phys. Res. **B 70**, 286 (1992).
[20] A. Stolz *et al.*, Phys. Rev. **C 65**, 064603 (2002).
[21] V. Hlinka *et al.*, Nucl. Instrm. and Meth. in Phys. Res. **A 419**, 503 (1998).
[22] I. Tanihata *et al.*, Prog. in Theor. Exp. Phys., 043D05 (2016).
[23] W. Nörtershäuser *et al.*, Phys. Rev. Lett. **102**, 062503 (2009).
[24] L.V. Chulkov *et al.*, Nucl. Phys. **A 674**, 330 (2000).
[25] W. R. Webber, J. C. Kish, and D. A. Schrier, Phys. Rev. **C 41**, 520 (1990).
[26] Y. Suzuki *et al.*, Phys. Rev. **C 94**, 011602(R) (2016).
[27] Y. Kanada En'yo, Phys. Rev. **C 91**, 014315 (2015).
[28] M. Kimura, *private communication.*
[29] A. Ekström *et al.*, Phys. Rev. Lett. **110**, 192502 (2013).
[30] W. Horiuchi *et al.*, Phys. Rev. **C 75**, 044607 (2007).
[31] T. Nakamura *et al.* Phys. Rev. Lett. **83** 112, (1999).
[32] M.K. Sharma *et al.*, Chin, Phys. **C 39**, 064102 (2015).
[33] R.J. Bartlett and M. Musiał, Rev. Mod. Phys., **79**, 291 (2007).
[34] J.R. Gour *et al.*, Phys. Rev. **C 74**, 024310 (2006).
[35] G. Hagen *et al.*, Rep. on Prog. in Phys. **77**, 096302 (2014).
[36] G.R. Jansen *et al.*, Phys. Rev. Lett. **113**, 142502 (2014).
[37] G.R. Jansen *et al.*, arXiv, nucl.-th 1511.00757, (2015).
[38] A. Ekström *et al.*, Phys. Rev. **C 91**, 051301(R) (2015).
[39] K. Hebeler *et al.*, Phys. Rev. **C83**, 031301 (2011).
[40] S.K. Bogner, R.J. Furnstahl and R.J. Perry, Phys. Rev. **C 75**. 061001 (2007).
[41] D.R. Entem and R. Machleidt, Phys. Rev. **C 68**, 041001 (2003).